Stress distributions and energetics in the laterally ordered systems of buried pyramidal Ge/Si(001) islands: An atomistic simulation study

Maxim A. Makeev,* Wenbin Yu, and Anupam Madhukar
Nanostructure Materials and Devices Laboratory, Departments of Materials Science and Physics, University of Southern California, Los Angeles, California 90089-0241, USA

(Received 26 November 2002; revised manuscript received 4 June 2003; published 3 November 2003)

Stress distributions in laterally ordered arrays of coherent Ge islands of shallow pyramidal shape buried in a Si(001) matrix are studied via large-scale atomistic simulations, using Stillinger-Weber Ge/Si systems as a vehicle. The existence of tensile hydrostatic stress regions is observed on the spacer surface, above the buried islands. Our previously reported finding [M. A. Makeev and A. Madhukar, Phys. Rev. Lett. **86**, 5542 (2001)] that the hydrostatic stress at the spacer layer surface above the island apex is nearly inversely proportional to the spacer layer thickness is validated by a comparison with experimental data. The *lateral* variations of the hydrostatic stress on the spacer layer surface show ''bell-shape'' profiles, with the effective size of the tensile regions above the island apex varying as a power law with the spacer layer thickness, with the power exponent being greater than 1. Studies of the energetics of twofold stacks of island systems show that the elastic interaction energy between the islands is minimized for the vertically aligned geometry. The spacer layer thickness dependence of the hydrostatic and biaxial stress field distributions in the *interior* of the Si(001) matrix are presented as these define the behavior of the electron and hole three-dimensional confinement potentials that determine the electronic properties of the pyramidal island quantum dots.

DOI: 10.1103/PhysRevB.68.195301 PACS number(s): 68.65.Hb, 81.10.Aj, 68.35.−p, 62.20.Dc

I. INTRODUCTION

Self-assembled three-dimensional (3D) coherent islands, formed in lattice-mismatched semiconductor heteroepitaxy, continue to be in the focus of active research due to their potential for technological applications in the fields of nanoelectronics and photonics.[1,2] The island formation is caused by the lattice-mismatch-associated stress-driven morphological instability that occurs during the growth of a heteroepitaxical film deposited on a substrate made of a material with a smaller lattice constant. The morphological evolution of the deposited film is generally observed to occur in the form of a Stranski-Krastanow (SK) growth mode, i.e., it proceeds by the formation of an essentially flat layer of thickness dependent upon the lattice mismatch, called the wetting layer (WL), followed by the formation of truly 3D coherent nanoscale islands of different (controllable) shapes such as pyramids or domes. When buried by the overgrowth of a suitable material, most often the same as the underlying substrate, such islands act as quantum dots (QDs). Because of their coherent nature, every individual QD possesses nearly perfect ''atomlike'' electronic and optical properties arising from the effective 3D confinement of carriers and excitons in such structures.[1] However, many potential device applications require a better island size and shape uniformity in the ensemble of QDs with a high spatial density. While improvements in the size and shape distribution of a single layer ensemble of islands has been realized via an innovative manipulation of the deposition process,[3] many device designs require multiple layers of island quantum dots.[1,2] One of the remarkable features of such multilayered systems is the tendency of the islands to self-organize in vertically aligned structures.[4,5] These systems have been proven to show not only a high degree of ordering in the vertical (i.e., growth) direction and increased size and shape uniformity, but also improved lateral correlations in the upper layers of such multilayered QD structures.

In recent years, extensive experimental and theoretical studies of vertically ordered multilayer systems of semiconductor QDs, for a number of materials, have been undertaken. By now, it is generally recognized that the stress and associated strain field evolution during the growth process and their steady-state distributions in such systems play important roles in defining structural and electronic characteristics of QD structures. Vertically self-organized (VSO) QD structures have been extensively examined in InAs/GaAs,[4–10] Ge/Si,[11–26] and $PbSe/PbEu_{1-x}Te_x$ systems.[27–30] Experimental studies of multiple stacks of InAs islands in GaAs, grown via molecular beam epitaxy, have been reported in Refs. 4 and 5. Using transmission electron microscopy, the authors have shown that, although the spacer layer surface morphology undergoes a planarization with growth, the buried islands induce inhomogeneous stress profiles on the spacer layer surface. The latter, in their turn, cause a stress-gradient driven bias for adatom diffusion during subsequent deposition, thus leading to the vertically correlated island growth.[5] A nearly perfect vertical correlation was observed for relatively small spacer layer thicknesses, while an uncorrelated regime was found to take place for sufficiently large spacer thicknesses.[5] An increased size uniformity accompanies the vertical stacking.[5,7,10] Similar studies of the vertically correlated systems of Ge/Si islands have been reported in Refs. 11–25. In Refs. 18 and 19, it was shown that the Ge wetting layer thickness of 3–4 ML for the first set of islands decreases with the number of deposited layers in the multilayer structure. Furthermore, a rather regular hexagonal ordering of QDs in the upper layers of the Ge/Si QD superlattice, accompanied by a narrowing of the island size distribution, has also been observed in

experiments.[19] Extensive experimental studies of vertically self-organized growth in PbSe/PbEuTe systems were reported in Refs. 27–30. It was shown that in PbSe/PbEuTe systems a fcc stacking takes place. This behavior has been attributed to the existence of elastic energy local minima on the spacer layer surface possessing threefold symmetry. These minima arise due to a high degree of elastic anisotropy in such materials.[27–30] Vertical *anticorrelation* in the systems of two-dimensional CdSe islands in ZnSe has been reported in Ref. 31. This striking result prompted further theoretical investigations of the multilayered VSO QD structures with the goal of building a unified theory of the phenomenon of vertical self-organization.

The importance of understanding the stress and associated strain field effects in systems of multilayered heteroepitaxical islands has led to the development of the necessary theoretical tools. Conventional small-strain continuum elasticity theory has been employed to investigate the stresses and strains in the equilibrium structures of the uncovered (''free-standing'') SK islands.[1] A number of theoretical descriptions of the VSO QD systems have been also based on continuum elasticity models. Within the framework of these models, a single isolated island is generally treated as an embedded force dipole source (pointlike or of a spherical shape).[5,32,33] A finite element implementation of the continuum elasticity theory has also been used to study the stress fields in such systems.[34–37] These two approaches have been very helpful in gaining a qualitative understanding of various aspects of stress behavior in the multilayered QD structures. It has been shown that a buried island induces a region of tensile stress on the spacer surface above its apex, which favors a vertically correlated growth in the successive layers of QDs.[5,32,33] An increased size uniformity through the columns of the multilayered QD structures is a natural outcome.[32,33] Further, a theoretical approach that describes different regimes in the QD multiple layer structure formation was developed in Refs. 38 and 39. It was shown that the elastic anisotropy of the matrix material gives rise to an oscillatory behavior of the strain field with the spacer layer thickness, thus leading to the possibility of both correlation and anticorrelation in such systems.[38,39]

Atomistic simulations have been proven to successfully complement the continuum elasticity based approaches, providing a microscopic description of the stress and strain field behavior. Several studies of the atomic-level stresses in both uncovered (''free-standing'') (Refs. 40 and 41) and covered[40,42–46] Ge/Si islands have been performed. Some results of our study were previously reported in Ref. 45. Here, we expand the scope of discussion to various aspects of stress relaxation in the buried QD systems and compare our results with the predictions of the linear elasticity theory based models and experimental data. We concentrate primarily on the effects of the spacer layer thickness on the stress relaxation, and discuss the implications of this behavior for the multilayer structure formation. The effect of strain on the electronic properties of such materials is also discussed.

The remainder of the paper is organized as follows. In Sec. II, we describe the methodology of the simulations. Section III is dedicated to the results of our studies of the spacer layer morphology. A short overview of the analytical models, describing the stress fields induced by buried pointlike and extended objects in an elastic media is given in Sec. IV. Next, in Sec. V, we present our simulation results on the behavior of the stress at the spacer surface in the two-dimensional surface plane (Sec. V A) and above the island apex as a function of the spacer layer thickness (Sec. V B). Further, in Sec. VI, we present the results of our studies of the energetics of the two-layer Ge/Si island systems. Then, in Sec. VII, we discuss the stress field distributions in the Si(001) matrix surrounding the embedded Ge islands. The emphasis is on the hydrostatic and biaxial stress field dependencies on the spacer layer thickness, as these control the three-dimensional quantum dot confinement potentials arising from the conduction and valence band edge discontinuities between the island and surrounding matrix material. Finally, we summarize our principal results in Sec. VIII.

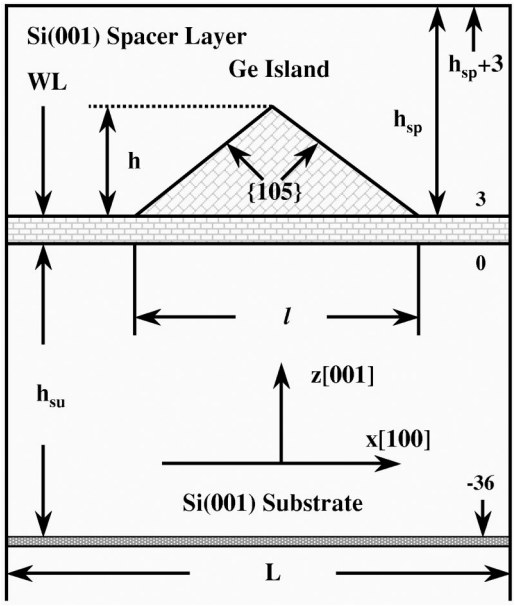

FIG. 1. Schematic illustrating the modeled system. Germanium island of height h (with WL of 3 ML underneath) is positioned on a Si(001) substrate of thickness h_{su} and covered by a Si(001) spacer layer of thickness h_{sp}. The lateral size of the simulation box, $L = 60a_{Si}$, and the lateral island size is l. Here a_{Si} is the lattice constant of crystalline Si, $a_{Si} = 5.43095$ Å. Numbers correspond to the z coordinate of the atomic planes, measured in ML, N_z.

II. SIMULATION METHODOLOGY

A. Simulation system

A schematic illustrating the cross-sectional geometry of the simulation system is shown in Fig. 1. The simulation system consists of an $h_{su} = 37$ ML thick Si(001) substrate; a $\langle 100 \rangle$ oriented square base and $\{105\}$ side facets bound[47] pyramidal Ge island of height h and base length $l = 40a_{Si}$ (a_{Si} being the Si(001) surface lattice constant) is positioned on a 3-ML Ge WL. The island is covered by a Si(001) spacer layer of varied thickness h_{sp}. At the bottom, 3 ML of the Si(001) substrate are fixed to the bulk Si(001) lattice constant

and the rest of the atoms are allowed to relax. The Si(001) spacer layer surface is dimerized, with dimers oriented along the $[1\bar{1}0]$ direction. The initial configuration is built as follows. All the atoms are placed in the Si(001) bulk crystalline positions. The spacer surface atoms are shifted by $0.05 \times a_{Si}$ towards each other in pairs to provide an onset for dimerization. Periodic boundary conditions are applied in the x and y directions to the simulation cell of size $L=60a_{Si}$, thus mimicking an infinite layer of Ge QDs in Si(001), separated by a distance L. The system is relaxed to the minimum of the potential energy configuration using a conjugate gradient minimization algorithm. The relaxation proceeds until the net force, acting on each atom, does not exceed 10^{-4} eV/Å.[48] All the relevant quantities, such as stresses, atomic displacements, and the elastic energy of the system, are calculated for such an equilibrium configuration.

A number of interatomic potentials for various forms of silicon has been developed in the past. A comprehensive review, discussing nearly all of such potentials, is available in Ref. 48. In the present work, we employ the SW functional form of the potential to model interatomic interactions between both silicon and germanium atoms.[49] The potential energy of an atom, interacting with the others via the SW potential, $\Phi(\mathbf{r}_i)$, consists of a sum of the two- and three-body contributions and is represented by the following functional form:

$$\Phi(\mathbf{r}_i)=\sum_{i<j} \epsilon f_2(\mathbf{r}_{ij})+\sum_{i<j<k} \lambda f_3(\mathbf{r}_i,\mathbf{r}_j,\mathbf{r}_k). \qquad (1)$$

Here, f_2 is the two-body interaction term, while f_3 accounts for the three-body interactions, which stabilize the tetrahedral (zinc-blende) structure of the crystalline Si and Ge; ϵ is the depth of the local potential profile. The functional forms of f_2 and f_3 as well as the parameters of the interaction potential for Si atoms are taken from the original paper by Stillinger and Weber.[49] We note that Stillinger and Weber obtained the values via a fitting to the experimental properties of the diamond-cubic (dc) and molten phases of silicon. Several choices of parameters for the interatomic potential of Ge have been previously suggested in the literature.[50–52] In our calculations, we adopt the model parameters derived by Ding and Andersen.[50] The interatomic interactions between Si and Ge are calculated using the potential with the functional form the same as Eq. (1), but with rescaled parameters: $\epsilon_{Si-Ge}=(\epsilon_{Si}\epsilon_{Ge})^{1/2}$, $\lambda_{Si-Ge}=(\lambda_{Si}\lambda_{Ge})^{1/2}$ and $\sigma_{Si-Ge}=(\sigma_{Si}+\sigma_{Ge})/2$.[50] In all cases, the potential function [Eq. (1)] was modified to ensure that the potential and its first derivative go to zero at the predetermined cutoff distance $R_c \simeq 1.80\times\sigma_{Si(Ge)}$. Despite the fact that potential of the form Eq. (1) contains intrinsically three-body terms, it can be shown that this contribution is decomposable into a sum of two-body terms so that the actual calculations of the three-body terms can be avoided. The potentials for both Si and Ge have been proven to provide a satisfactory description of the structural and mechanical properties of the bulk materials (such as the phonon density of states and elastic modulus) as well as to give a correct (2×1) surface reconstruction for both Si and Ge surfaces. Remarkably, as a comparison with the first principles electronic structure calculations show, these potentials are also quite adequate in a description of the surface energy, and the surface stress anisotropy, computed with these potentials, agrees well with the existing experimental results. Moreover, a recent study by Kikuchi *et al.* has shown that the SW potential is better suited for the purposes of atomistic strain calculations in the Ge/Si QD systems as compared to the valence field force model with the Keating potential, also often used in the literature.[43]

B. Atomically resolved stress calculation

The recent progress in computer performance and the extensive development of advanced computing techniques for large scale simulations has made it possible to obtain atomistically resolved information on systems comprised of millions of atoms. Thus, modern molecular dynamics (MD) based atomistic simulation techniques now allow for calculating atomically resolved stresses and strains in the model systems with sizes approaching the dimensions of the real ones: This is particularly true for the nanostructured materials. A number of methodologies for atomically resolved stress calculations have been previously proposed in the literature.[53,54] Following Ref. 53, we calculate the quantity given by the following expression:

$$\sigma^i_{\alpha\beta}=-\frac{1}{\Omega}\left(\frac{p_i^\alpha p_i^\beta}{m_i}+\frac{1}{4}\sum_j (r_{ij}^\beta f_{ij}^\alpha + r_{ij}^\alpha f_{ij}^\beta)\right). \qquad (2)$$

Here, m_i and p_i are the mass and the momentum of an atom i, $\mathbf{r}_{ij}$ is a vector connecting atoms i and j, f_{ij} is the force acting on atom i due to an atom j, α and β denote the Cartesian components of the coordinate system, and Ω is an average atomic volume. (For discussion purposes, we refer to the quantity $\sigma^i_{\alpha\beta}$ as the atomistically-resolved stress tensor, although it is unlikely to be the quantity measured in experiments, where a coarse graining over some larger volume than Ω is inherent.) Following this convention, a tensile stress corresponds to the positive sign and a compressive stress to the negative sign. This choice provides a clear correspondence between the positive tensile stress and strain of a locally expanded (as compared to the lattice constant of the bulk material) lattice, while the negative compressive stress corresponds to a locally shrunk (as compared to the lattice constant of the bulk material) lattice. We note that, in our simulations we assume that the spatial variations of the average atomic volume can be neglected, and that Ω is constant throughout the system. Indeed, the average atomic volume variation in the system of Ge islands in Si, similar to those studied in the present work, has been recently investigated using MD simulations.[42] It was found that such variations, indeed, can be considered to be negligible (largest deviations being $\simeq 1\%$).

III. MORPHOLOGY OF THE SPACER LAYER SURFACE

In the process of the overgrowth of a lattice-mismatched material on the islands (i.e., during spacer layer deposition), the morphology of the spacer layer surface undergoes significant changes. Detailed investigations of the spacer surface

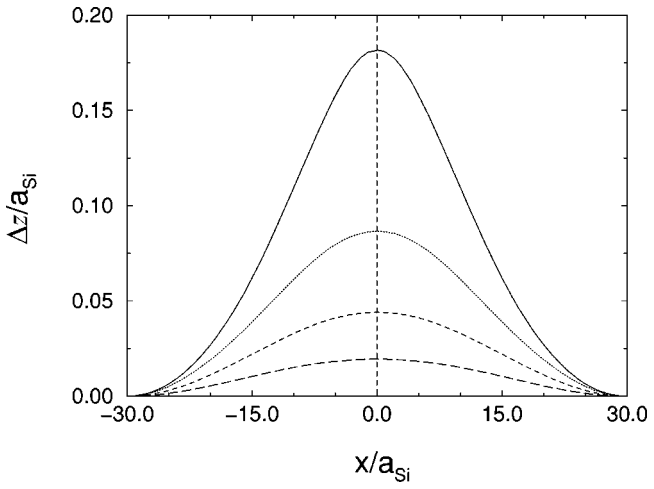

FIG. 2. Relative surface morphology undulations, $\Delta z/a_{Si}$, induced by island of base $l=40a_{Si}$ and height $h=17$ ML, are plotted along the lateral x direction on the spacer surface for four different spacer layer thicknesses: (a) $h_{sp}=29$ ML (solid line), (b) $h_{sp}=49$ ML (dotted line), (c) $h_{sp}=65$ ML (dashed line), and (d) $h_{sp}=81$ ML (long-dashed line). Relative atomic displacements are measured with respect to the crystalline bulk Si(001) lattice positions.

morphology evolution, during the overgrowth in InAs/GaAs systems, have been reported in Ref. 4. Using cross-sectional transmission electron microscopy, the authors have found that, in the initial stages of the overgrowth (i.e., for small spacer layer thicknesses), a substantial modulation of the spacer surface takes place. As the growth continues, however, the amplitude of these modulations decreases rapidly; the morphology of the spacer surface planarizes with growth. The implications of this behavior for the mass transport on the spacer surface has been discussed within the framework of a mechanochemical potential based model of adatom migration.[4] It was pointed out that, in general, two factors influence the adatom diffusivity on the spacer surface: one is the surface curvature driven diffusion, with the particle current proportional to the local surface curvature,[55] and the other is the stress-gradient driven diffusivity leading to mass transport from regions of the higher stress gradients to the lower ones. The latter has been found to be the dominant factor in the spacer layer surface profile evolution.[4] Furthermore, in Ref. 5, the surface mechanochemical potential model has been used to explain the process of spatially preferential initiation of islands on a morphologically planar spacer surface profile. Although no dominant surface curvature effects are present in these spacer layers, it is instructive to examine the nature of the spacer layer surface atomic displacements that accompany the surface stress.

In Fig. 2, we show the Si spacer layer surface atomic displacements Δz (calculated with respect to the bulk crystalline Si(001) positions) in the z direction for an array of buried Ge QDs of $h=17$ ML and $l=40a_{Si}$. The islands are covered with spacer layers of different thicknesses, h_{sp}. The largest upward displacements of the surface atoms are observed in the region above the island apex. They decay, however, rapidly away from the system center. In the regions between the islands these displacements become nearly negligible. At the point above the island apex, the largest displacement magnitude, $\Delta z\simeq 0.9$ Å, is observed for the smallest spacer layer thickness (see the $h_{sp}=29$ ML case). As the spacer layer thickness grows, however, the maximum displacements decrease in magnitude rapidly. Even for relatively thin spacer layer thicknesses (for instance, $h_{sp}=49$ ML, ~ 3 times the QD height), the maximum undulations become small as compared with the interplanar distance of bulk Si(001) ($\simeq 1.36$ Å). Moreover, the magnitude of undulations drops to a negligible value of $\simeq 0.1\%$ already for spacer layer thickness of $h_{sp}\simeq 81$ ML ($\simeq 10$ nm). This value is much smaller than the typical spacer thickness ($\simeq 25$ nm) used in experiments. The observed variations of the surface undulations are very slow. All of the above suggest that the curvature driven diffusivity can, indeed, be considered just as a minor corrective term in the stress driven self-organization. Consequently, in the following we concentrate mainly on the stress and associated strain field distributions as the major factors defining the mechanism of vertical self-organization and impacting on the electronic properties of Ge/Si QD systems.

IV. ANALYTICAL THEORIES OF THE STRESS FIELDS FROM ISLANDS

From the continuum elasticity perspective, a buried island has been considered as a dilatational center (pointlike or extended) in an isotropic elastic media. The precise geometry of the inclusion, adopted in different models, varies from pointlike to pyramidal. While inclusions of realistic shape are usually treated using finite element (FE) calculations, analytical models, based upon pointlike and/or spherical inclusion approximations, have been also suggested in the literature to model the systems of the buried lattice-mismatched islands.[5,12,32,33,37,39,56] The common approach to a solution of the problem of the elastic field from a point and/or extended imperfection in crystals is based upon the assumption that such features can be modeled in terms of double forces (with or without moments) in the semi-infinite elastic media.[57–59] The displacement fields in the surrounding media (as well as the stress and strain fields) then decay as $1/r^3$ with the distance from the center of an imperfection.[57–63] The finite size inclusions were considered mainly in the context of thermoelastic effects in composite materials. It was shown, however, that the temperature gradient in the composite elastic material can be modeled in terms of a distribution of dilatation centers of a particular strength.[64] Finite size spherical thermal inclusion in the elastic media was considered in Ref. 62. It was shown that the displacement (the stress and strain) fields demonstrate a functional dependence similar to that in the case of pointlike sources. In the case of finite-size spherical inclusion, the strength of the dilatation center is directly proportional to the inclusion volume and to the difference between the differential thermal expansion coefficients of two materials. A generalization of this approach to the lattice-mismatched inclusion of elliptical shape was made by Eshelby.[65] Among other things, he suggested a simple way to calculate the strength of

the dilatation center, easily adaptable for lattice-mismatched systems: the so-called ''sphere-in-hole'' model. Subsequently, finite size parallelepipedic thermal inclusions were considered by Hu,[66,67] who obtained stress and strain field dependences on the coordinates different from the functional dependences derived for the case of inclusions with spherical symmetry. In all the above mentioned models, the differences between the elastic coefficients of the host material and inclusion, as well as elastic anisotropy of crystal lattices, have been neglected. In the following, we refer to all models adopting the spherical symmetry of an inclusion as ''force-dipole'' approximation. The analytical form for the hydrostatic stress due to a spherical inclusion was reported in Refs. 61 and 66 to be

$$\mathrm{Tr}(\sigma)=\frac{4\Gamma G(4-8\nu)}{r^3}\left(1+\frac{3}{2r^2}\times\left[\frac{(4\nu-4)}{(4-8\nu)}(x^2+y^2)+\frac{8\nu}{(4-8\nu)}z^2\right]\right), \tag{3}$$

where $r=\sqrt{(x^2+y^2+z^2)}$, Γ is the strength of a dilatation center, given by $\Gamma=\epsilon_o V[(1+\nu)/(1-\nu)]$, ν is the Poisson ratio G is the shear modulus, V is the volume of the inclusion and ϵ_o is the coefficient characterizing the lattice-mismatch between the matrix material and the inclusion. The above expression for the dilatation strength has been suggested by Eshelby using the simplified model of a spherical inclusion with radius $(1+\epsilon_o)r_o$ embedded in a spherical cavity in the matrix with radius r_o (the ''sphere-in-hole'' model).[65] We have shown[68] that the analytical form [Eq. (3)] well describes the elastic stress fields from a *finite-size* spherical Ge inclusion in Si(001). This indicates that the elastic anisotropy of the crystal lattice, naturally incorporated in the simulations, does not much impact the basic qualitative conclusions on the inclusion-induced stress field behavior in the elastic media. Moreover, the assumption of a linear response works well for the Si/Ge systems (lattice mismatch $\simeq 4\%$). On the other hand, no exact closed-form analytical solution of the elasticity problem for a system of pyramidal shape misfitted buried islands, with the WL underneath and with a free surface nearby (as relevant to the experimental systems), has yet been reported. Thus, the question of the adequacy of the simplified analytical models for accurately representing the systems of singlelayered and multilayered pyramidal island QD structures remains open. In the following, we shed further light on this aspect through simulation results that augment previously reported findings. We also provide evidence from reported experimental results that confirm our previously reported nearly inverse linear dependence of the spacer layer surface stress above the pyramidal island apex as a function of the spacer layer thickness.

V. BURIED ISLAND INDUCED SPACER SURFACE STRESS

A. Lateral variations

The strain associated with a misfitted Ge QD embedded in a Si matrix ($\simeq 4\%$ lattice mismatch) is subject to a partial elastic relaxation. It is known[5,32,33] that this relaxation in the arrays of buried islands is responsible for the inhomogeneous stress profiles on the spacer layer surfaces. The regions of the Si matrix above the island apex and at the Si(001) spacer layer surface exhibit tensile stress. On the other hand, the stress in the region between the islands is compressive.[5,12,32,33] In the successive layers of the multilayered system, the islands tend to form in the region of tensile stress, thus leading to vertically correlated structure formation. The degree of vertical correlation is a function of the spacer layer thickness.[5] The size of the newly formed island is dependent on the width of the tensile region. We thus investigate these two factors. In the ideal case, a simple albeit realistic analytical model should be developed which allows estimations of both the stress magnitude and spatial profile for systems with different spacer thicknesses. Up to now, several approaches adopting continuum elasticity based models have been suggested in the literature.[5,12,32,33,37] Using the ''force-dipole'' approximation, in Refs. 5, 32, and 33 the authors have shown that a buried island induces a region of tensile stress on the spacer layer surface above the island apex. Subsequently, Monte Carlo simulations of the multilayered QD growth have been performed.[56] These have shown that the presence of the buried islands (approximated as subsurface force dipole stressors) induce a vertical correlation between the on-surface islands and the centers of symmetry of the buried stressors. The degree of correlations was found to be strongly dependent on the stressor depth, the incoming ion flux, and the growth temperature as in the mechanochemical potential based analytical model of Ref. 5. Below, we discuss the lateral stress variations on the spacer surface and compare the obtained results with the predictions of the continuum elasticity theory based models.

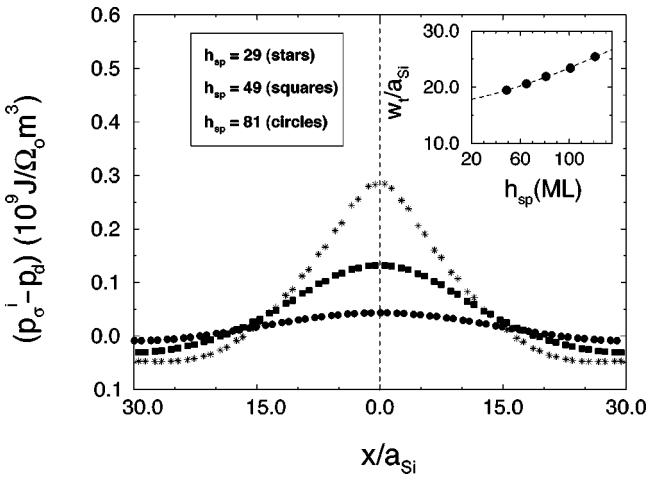

FIG. 3. Normalized hydrostatic stress (p^i_σ-p_d) variations along the lateral x direction on the spacer layer surface are shown for three different spacer layer thicknesses as indicated. Here, p_d is the stress associated with surface dimerization $p_d=0.747\times10^9$ J/$\Omega_o m^3$, where $\Omega_o=\Omega/a^3_{Si}$. The inset shows the width of the tensile stress region on the spacer surface, w_t, as a function of h_{sp} (solid circles). An analytical power law fit of w_t (see the text) is shown by the dashed line.

In Fig. 3, we show the spacer surface hydrostatic stress,

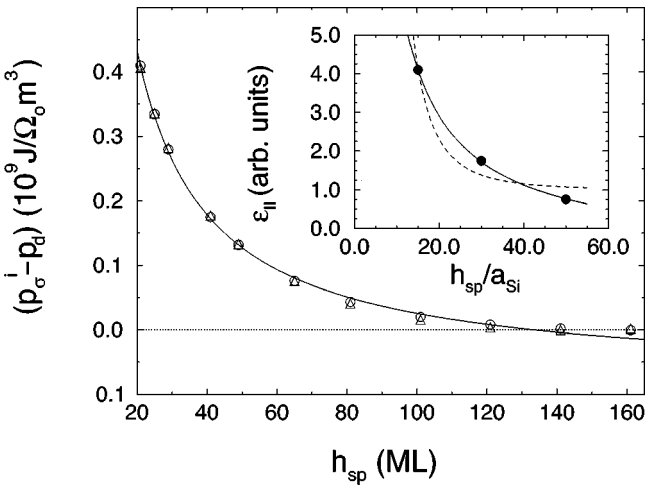

FIG. 4. Normalized hydrostatic stress (p_σ^i-p_d) on the spacer surface (open circles) at the point above the island apex, is plotted as a function of the spacer layer thickness, h_{sp}, measured in ML. The solid line shows the $p_\sigma^i(h_{sp})$-$p_d = -0.07 + 10.21/h_{sp}$ fit. The fit using an oscillatory function (see the discussion in the text) is shown by open triangles. The inset shows experimental data on the strain dependence of the in-plane strain on the spacer layer thickness h_{sp}, taken from Ref. 20 (solid circles). The solid line is the inverse linear fit, while the dashed line shows the $1/h_{sp}^3$ fit.

$p_\sigma^i = \mathrm{Tr}(\sigma) = [\sigma_{xx}(i) + \sigma_{yy}(i) + \sigma_{zz}(i)]$, variations in the lateral x direction for systems with three spacer layer thicknesses of 29, 49, and 81 ML for the $l = 40a_{Si}$ and $h = 17$ ML islands. The calculated quantity, however, requires a normalization at the surface, due to the existence of the surface reconstruction effects. We note that, for the 2×1 reconstructed surface, the atomic hydrostatic stress on the surface caused by the surface dimerization, p_d, is uniform and equal to $\simeq 0.747 \times 10^9$ J/$\Omega_o m^3$, where $\Omega_o = \Omega/a_{Si}^3$. Thus, merely to study the effect of the buried island, we normalize the hydrostatic stress by deducting the contribution coming from the surface dimerization, i.e., in Fig. 3 we plot (p_σ^i - p_d) as the relevant quantity. In all considered cases, the stress distributions have a ''bell-shape'' topology, with two distinct regions. The first region corresponds to a tensile stress domain centered at the buried island apex. The second region corresponds to a mildly compressive stress domain observed between the island and its images. The transition between the two regions is rather smooth. Within the compressive domain, the magnitude of the stress decreases with the distance from the center of the system. It does not, however, go to zero at the system borders due to the island-island elastic interactions. For an isolated buried island, the elastic stress field decays to zero for large lateral distances from the island. Thus, as a function of the island-island separation, the stress profiles should exhibit a minimum in the region between the islands as opposed to the nonzero compressive stress at the system boundary observed in Fig. 3. This behavior of the hydrostatic stress has been observed in our previous simulations[45] for systems with smaller island sizes or larger separation distances [see Ref. 45, Fig. 4 (inset), $L = 100a_{Si}$ case]. The variations in the spacer layer thickness affect both the magnitude of the hydrostatic stress on the surface and the lateral width of the tensile region. The stress magnitude decreases rapidly with the spacer thickness and the shape of the curve becomes flatter with increasing h_{sp}. A detailed account of the hydrostatic stress dependence on h_{sp} is given in Sec. V B. Here, in Fig. 3 (inset), we show the width w_t of the lateral stress region on the spacer layer surface as a function of the spacer layer thickness. We find that it approximately follows a $\sim h_{sp}^{1.4}$ dependence. Thus, the $\sim\sqrt{2}h_{sp}$ behavior of the lateral stress region width, predicted by Eq. (3) within the framework of the analytical models, does not find a rigorous confirmation in the regime simulated by our computer experiments. In fact, this dependence turns into $\sim h_{sp}^3$ for small spacer layer thicknesses. Note that the system we consider is not an individual isolated buried island, but rather a laterally ordered array of elastically interacting islands. For values of h_{sp} shown in the Fig. 3 (inset), however, these elastic interactions are likely to be small, and thus the deviations from the linear behavior of the analytical model of isolated inclusion are unlikely be due merely to the effect of elastic field coupling. Furthermore, our attempt to fit the simulation stress data with Eq. (3) does not give a satisfactory result if all the fitting parameters are to retain their intrinsic physical meaning. For instance, the fitting value of the dipole strength Γ in Eq. (3) required considerable changes in the three spacer layer thicknesses. We are, however, able to reproduce very well the ''bell-shape'' topology of the stress profiles on the spacer layer surface, if the parameters in Eq. (3) are considered not to be constrained by any physical considerations.

B. Spacer surface stress dependence on the spacer thickness

The degree of the vertical correlation in multilayers of strain-driven island QDs has been shown to depend strongly on the spacer layer thickness.[5,12,21] In general, depending on the thickness of the spacer layer, three different regimes can be distinguished. The first regime corresponds to small values of h_{sp} and is characterized by a nearly perfect degree of the vertical correlations. In the second regime, a transition between the perfect vertical correlation and a random positioning on the spacer layer surface takes place. This regime corresponds to intermediate spacer layer thicknesses. For large values of h_{sp}, the probability to find vertically correlated islands is nearly zero. As a mechanism of vertical self-organization during the growth of multilayer structures, a model, based on the stress driven diffusion of individual adatoms, has been suggested in Ref. 5. Such a view focuses on the real-time phenomena of growth and the significance of the kinetics of surface migration of adatoms that contribute to a system moving towards, at least locally, a thermodynamic ground state, but does not rely upon the system always reaching the perfectly ordered state implied by a description based on purely minimum energy considerations (see Sec. VI). The model of Ref. 5 deals with the probability of vertical pairing, and thus accounts for the influence of the spacer surface stress magnitude and lateral range through the control of real growth parameters such as the adatom flux from vapor and substrate temperature. In Ref. 12, the authors con-

clude that this coupling cannot be sufficiently strong to account for the observed interisland vertical correlations. Their estimates, however, are based upon the assumption that the stress and the associated strain fields of an individual island can be described in terms of the h_{sp}^{-3} dependence derived for a force dipole source in the elastic media. In a previous publication (see Ref. 45), we have shown, however, that the hydrostatic stress on the spacer surface, from an ordered array of {105} sidewall (shallow) Ge islands in Si, follows a nearly $1/h_{sp}$ dependence with the spacer layer thickness. In the following, we further our discussion of the hydrostatic stress behavior. Thus, in Fig. 4, we show the atomically resolved surface hydrostatic stress p_{σ}^{i} at the point above the buried island apex (circles) as a function of spacer layer thickness, h_{sp}. It decreases monotonically as a function of h_{sp} following approximately a $p_{\sigma}^{i}=-0.07+10.21/h_{sp}$ functional dependence. This behavior is rather robust for both small and intermediate values of the spacer layer thickness, h_{sp}. Additionally, the biaxial stress at the spacer layer surface also exhibits an inverse linear dependence on h_{sp} (see Sec. VII). On the other hand, in the limit of large h_{sp}, the spacer surface hydrostatic stress above the island apex turns mildly compressive (see, for example, $h_{sp}=160$ ML). In Ref. 39, a theoretical model was developed that allows for stress sign oscillations with h_{sp}. Recently, in Ref. 46, the author reported on simulations of pyramidal islands with facets oriented at 45° with respect to the z axis (i.e., much steeper than the $\simeq 11.3°$ slope of our {105} side-facet islands) and also found an approximately $1/h_{sp}$ behavior. This extends the applicability of our earlier finding[45] beyond the {105}-faceted islands. Moreover, Ref. 46 found an oscillatory behavior of the stress field. As was suggested in Ref. 39, the period of oscillations of the stress function in Ref. 46 is defined by the interisland separation distance. The steeper islands and stronger island-island interactions in the simulations of Ref. 46, we suggest, underlies the clearer manifestation of oscillations as compared to our results from shallower islands. We have fitted our simulation data to the function $p_{\sigma}^{i}=(a_1+a_2/h_{sp})\cos(a_3+2\pi h_{sp}/a_4)$, where a_i $(i=1-4)$ are the fitting constants (triangles). We find that this fitting is in excellent agreement with our simulation data. The parameters a_1 and a_2 are found to match closely the ones obtained for the inverse linear fit (solid line). Moreover, the value of parameter a_4 confirms the assertions contained in Ref. 39. Note, however, that we have observed only transitions to the region of negative stresses, with the absolute values of the stresses being very small. Thus, it does not seem to be reasonable to extend the simulations for larger values of h_{sp}, to test the assumptions of Ref. 39. On the other hand, in Ref. 46 the author has succeeded in obtaining two periods of oscillations. We also note that the above mentioned oscillations arise due to the elastic anisotropy of the crystal lattice and, normally, should not lead to a new morphological regime in Ge/Si systems (i.e., anticorrelation). This is due to small anisotropy in Si/Ge, as compared, for instance, with CdSe/ZnSe systems. In the latter case, an anticorrelated growth has been observed experimentally.[31]

Recently, an experimental investigation of the strain field behavior in the multiple layers of self-assembled Ge/Si islands has been carried out by Schmidt and Eberl.[20] The authors reported on the WL related photoluminescence (PL) transition energy shifts of different WLs in systems of n layers of Ge QDs $(n=1-7)$, separated by Si spacer layers of varying thicknesses. The behavior of the observed separation between different WL PL peaks as a function of n and spacer layer thickness was analyzed based upon the assumption that such an energy separation is proportional to the in-plane strain at the spacer surface. The results are presented in Fig. 5 of Ref. 20, that gives $\epsilon_{||}$ values for three spacer thicknesses of 15, 30, and 50 nm, all extracted from the relation, $\Delta E_{wl}=(E_{wl1}-E_{wl2})=C\epsilon_{||}(z)$, in which E_{wl1} and E_{wl2} are the measured PL peak energies of the first and second wetting layers and C is a fitting constant. We have plotted the values of the extracted strains from the data of Fig. 5 of Ref. 20 as a function of the spacer thickness in Fig. 4 inset (circles). The solid line in the inset shows a fit of the $1/h_{sp}$ dependence obtained from our simulations.[45] On the other hand, an attempt to fit the experimental data with the $1/h_{sp}^{3}$ dependence (dashed line in the inset of Fig. 4) seems to be inadequate.[69] We note, however, that there are still open issues concerning the fitting parameters and their connection to the physical properties of the system. An attempt must be made to develop an analytic theory of the stress field from a single buried pyramidal island with a WL underneath to understand all the aspects of the problem.

Note that our result on the spacer thickness dependence of the hydrostatic stress has one rather important implication. The central quantity describing the island-island correlation is the correlation probability which has been analytically computed in Refs. 5 and 12, employing the h_{sp}^{-3} dependence of the hydrostatic stress on the basis of the assumed spherically symmetric point-like dipole force model. The authors of Ref. 12, in analyzing their experimental data, were led to conclude that the interaction energy is not sufficient to account for stress-driven adatom diffusivity. As our results here show, however, the buried island induced elastic stress field behaves as h_{sp}^{-1} and is significantly stronger. This implies that in Ref. 12 the buried island induced stress coupling leading to adatom diffusion bias on the spacer surface is significantly underestimated due to the much shorter ranged h_{sp}^{-3} decay behavior employed.

VI. ENERGETICS OF THE ISLAND SYSTEMS

In Sec. V, we have shown that a buried Ge island in the Si(001) matrix induces a tensile stress domain on the spacer layer surface, with the maximum of the stress distribution function above the buried island apex. Such tensile stress regions are favorable for the successive layer island formation.[5,32,33] To investigate the energetics of the island systems, in Fig. 5 we show the total energy difference (per atom), plotted as a function of the lateral displacement Δx from the position of perfect vertical correlation. We have simulated two systems of buried Ge islands, each of lateral size $l=40a_{Si}$ and height $h=17$ ML. The islands are positioned on the Si(001) substrate of thickness $h_{su}=37$ ML,

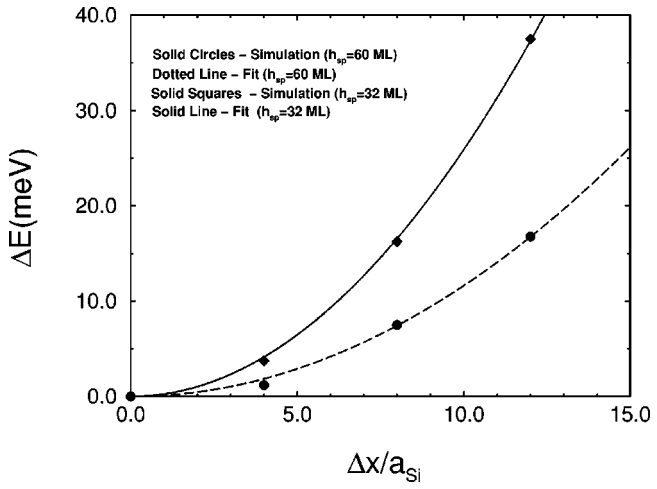

FIG. 5. The variation of the excess energy per atom, ΔE, as a function of the island's displacement Δx from the position of perfect vertical correlation. The system size is $L=60a_{Si}$, and the island dimensions are $l=40a_{Si}$ and $h=17$ ML. Values are shown for two spacer layer thicknesses: (a) $h_{sp}=32$ ML (solid squares) and (b) $h_{sp}=60$ ML (solid circles). The solid line shows the analytical $\simeq(\Delta x)^2$ fit for system (a), while the dashed line represents a similar fit for (b).

and covered with spacer layers of two different thicknesses: (1) $h_{sp}=32$ ML and (2) $h_{sp}=60$ ML. In both cases, the second layer of Ge islands (of the same lateral sizes and height) has been positioned on the undimerized Si(001) spacer layer surface, with a 3-ML-thick Ge WL underneath. The standard minimization procedure is performed in each case to find the atomic configuration corresponding to the minimum of the total potential energy (note that we consider zero temperature case). Initially, the simulations were performed for a system with perfectly vertically aligned islands ($\Delta x=0$). We denote the total potential energy of this configuration as E_o. Next, the simulations were done for systems where the lateral positions of islands in the second layer are shifted by a factor Δx from the position of perfect vertical correlations. The new total potential energies, $E(\Delta x)$, corresponding to such configurations were calculated. The energy difference between the two configurations, $\Delta E=E(\Delta x)-E_o$, is exactly the lateral displacement dependent energy excess due to the lateral misalignment. In Fig. 5, we show the total energy difference ΔE computed for four different values of lateral misalignment, Δx, ($\Delta x/a_{Si}=0,4,8,12$) and for two spacer layer thicknesses: (1) $h_{sp}=32$ ML (filled squares) and (2) $h_{sp}=60$ ML (filled circles). As one can see, for both systems, the total energy minimum corresponds to the configuration of perfect vertical alignment. As deviations from the position of perfect vertical correlations occur, ΔE increases rapidly with Δx, following approximately a $\sim\Delta x^2$ dependence. The Δx^2 fits for both simulated systems are shown in Fig. 5 by solid ($h_{sp}=32$ ML) and dashed ($h_{sp}=60$ ML) lines. As expected, the energy rise is larger for the system with a thinner spacer layer ($h_{sp}=32$ ML).

VII. STRESS DISTRIBUTION IN THE SI(001) MATRIX

In the previous sections we have presented results on the nature of the spacer layer surface morphology and stress due to the buried islands. In this section we present some results on the behavior of stress distribution inside the spacer matrix, in both *lateral and vertical* directions. The spatial distribution of the strain field in the close vicinity of QDs has a strong effect on the electronic properties of these systems, as these control the valence and conduction band alignments that define the confining potentials which give rise to the quantum dot nature of inclusions. (For a compound semiconductor they also give rise to the strain-induced piezoelectric effect.) The conduction band alignment is affected primarily by the hydrostatic strain, while the valence band edges are modified by both hydrostatic and biaxial strains. On the other hand, the piezoelectric effect in the systems is controlled by the *off-diagonal* elements of the strain tensor.

The effect of the strain is usually incorporated into the electronic structure calculations within the framework of a model originally developed by Bir and Pikus for homogeneously stressed semiconductors,[70] and further generalized in Refs. 71–74. Thus, in the idealized situation, the knowledge of the band-gap differences and the strain fields should provide complete information regarding the electronic states in the system of buried QDs. Electronic structure calculations have been performed for InAs/GaAs (Refs. 3 and 75–80) and Ge/Si (Refs. 81 and 82) systems of QDs of pyramidal (truncated pyramid) shape. The band alignments and the quantum confinement effects in the system of spherical Ge QDs in Si have been studied in Ref. 83. The stress and associated strain field distributions in the QD systems are, in general, a function of a set of parameters which include the spacer layer thickness, lateral and vertical dimensions of the islands, facet orientations, the average lateral separation distance between the islands in a row, the average distance between the QDs in the vertical direction, and a number of vertically self-organized rows of the islands. Thus, an adequate model for electronic structure calculations has to incorporate all these parameters self-consistently and, consequently, represent a rather complex problem. Moreover, *ab initio* calculations cannot, normally, be performed for systems of realistic sizes, due to the exceedingly large computational resources required. A complete knowledge of the stress and associated strain field variations with all of the parameters characterizing the system thus seems to be absolutely crucial for understanding the electronic structure of multilayer QD structures. In the following, we discuss the behavior of the hydrostatic and biaxial stresses in both the island interior and the surrounding Si(001) matrix, with a particular emphasis on the stress field dependence on the spacer layer thickness, h_{sp}.

Hydrostatic stress

To reduce the complexity of the problem, we consider only one row of buried Ge islands of the same size, weakly interacting with each other through their elastic fields, and concentrate mainly on the effects of the spacer layer thickness variations. We investigate the behavior of the hydrostatic, p_σ^i, and biaxial, $\sigma_b=[2\sigma_{zz}-(\sigma_{xx}+\sigma_{yy})]$, stresses in the systems of Ge islands embedded in a Si(001) matrix. Buried islands of size $l=40a_{Si}$ and $h=17$ ML, separated by

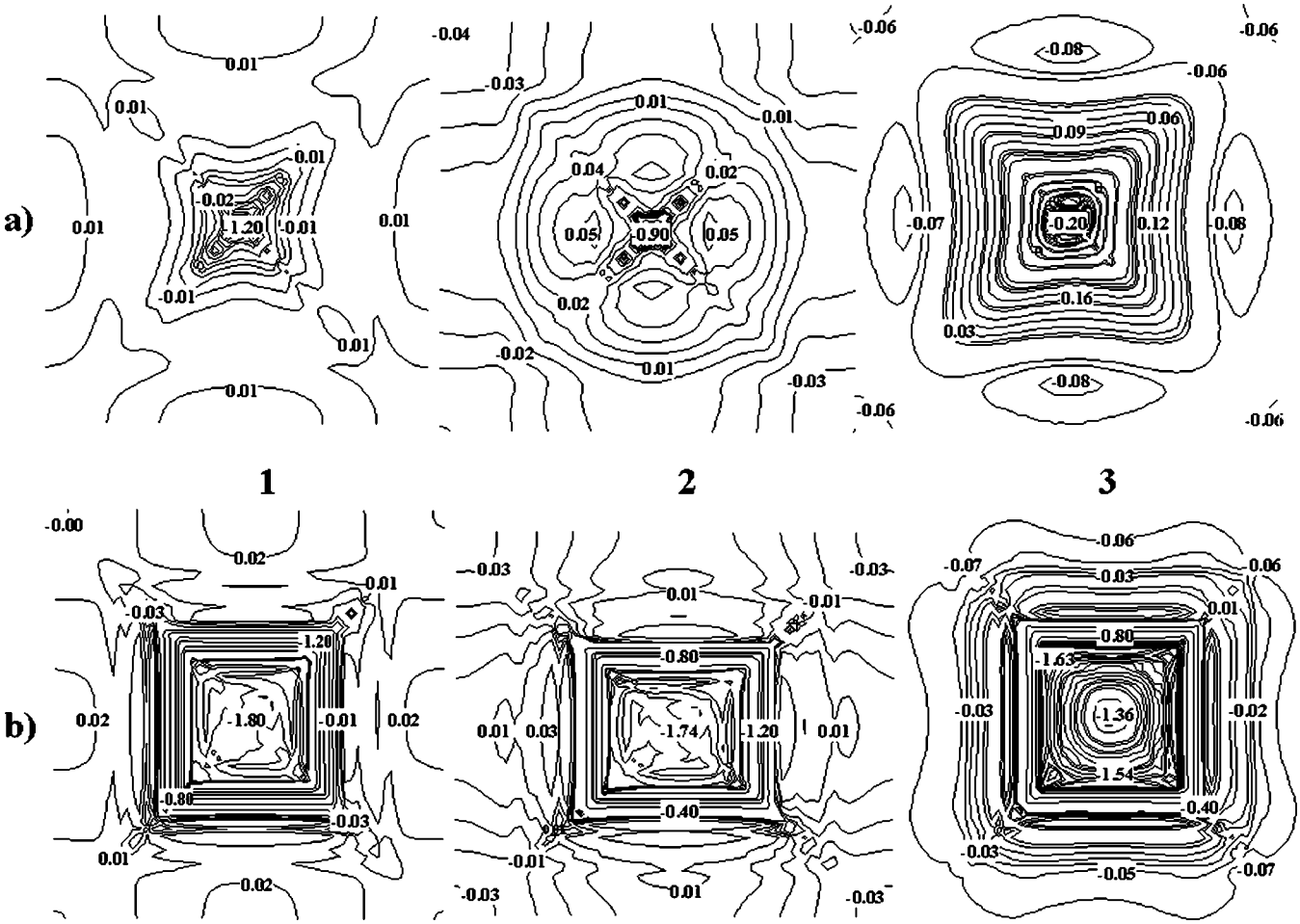

FIG. 6. Contour plots of the hydrostatic stress (in the units of 10^9 J/$\Omega_o m^3$) in the plane cutting through (a) the island apex and (b) the center of the island are shown for three different spacer layer thicknesses: (1) $h_{sp}=81$ ML, (2) $h_{sp}=49$ ML, and (3) $h_{sp}=21$ ML. Island height is 17 ML.

distance $L=60a_{Si}$, are considered, and different spacer layer thicknesses are employed. Limited information on the behavior of the hydrostatic stress in the vertical direction along a line passing through the island apex has been previously reported by us in Ref. 45. Below, we provide a more detailed discussion of the effects of the hydrostatic stress distribution, given its significance for defining the three-dimensional confinement potential for the conduction band states in quantum dots. But first we briefly recall from Ref. 45 that, depending on the spacer layer thickness, two different regimes of stress relaxation in the vertical direction can be discriminated in the system. For a spacer layer thickness close to the island's height, the hydrostatic stress along a line passing through the island base center and the apex is tensile in the substrate layer, changing rapidly in the Ge island interior to highly compressive and then turning tensile again in the vicinity of the spacer layer surface. As the spacer thickness grows, however, this tendency changes; the Si substrate becomes mildly compressive, while the island's interior becomes even more compressive. We note that the compressive stress domain in the island's interior does not relax with N_z as rapidly for large h_{sp}, as for small ones. In fact, for large values of h_{sp}, there is a compressive region of ~ 10 ML just above the island. With increasing h_{sp}, the tensile stress on the spacer layer surface above the island apex decreases in magnitude. Furthermore, for large values of h_{sp}, the Ge island's interior exhibits a compressive hydrostatic stress, which is nearly constant within the island size range examined here (and, as reported in Ref. 45, is equal to -1.75×10^9 J/$\Omega_o m^3$). Given that the conduction band edge shift is proportional to the hydrostatic stress, this would mean a nearly flat island conduction band-gap edge, for systems with large spacer thicknesses. For small spacer layer thicknesses, however, the hydrostatic stress relaxes towards the island apex by a factor of $\simeq -0.5\times 10^9$ J/$\Omega_o m^3$,[45] leading to corresponding variations in the band-edge behavior. The observed increase in the hydrostatic stress with the increased spacer layer thickness leads to an effective lifting up of the bottom of the potential well of the quantum dot conduction band. This, in turn, causes a reduction of the quantum confinement effects. Increasing hydrostatic stress will contribute similarly to the confinement potentials for the light- and heavy-hole bands. Next we provide results for the two-dimensional (i.e., in-plane) spatial distribution of the hydrostatic stress in a set of chosen planes parallel to the spacer surface for different spacer layer thicknesses.

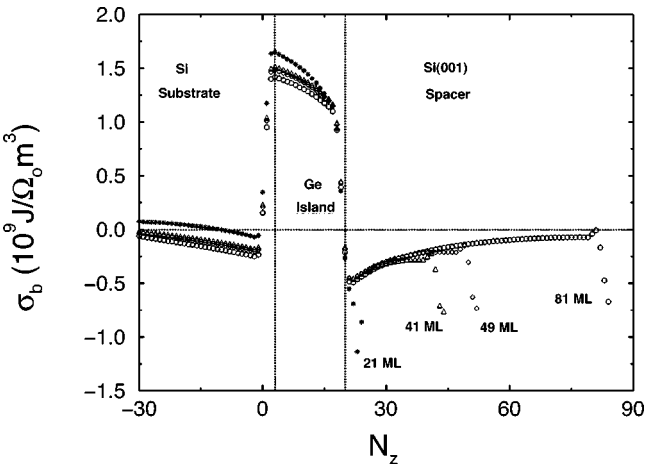

FIG. 7. The biaxial stress, σ_b, variations with the atomic plane number, N_z, are shown along the line passing through the island base center and the apex. Different curves are for different spacer layer thicknesses: (a) $h_{sp}=81$ ML (circles), (b) $h_{sp}=49$ ML (diamonds), (c) $h_{sp}=41$ ML (triangles), and (d) $h_{sp}=21$ ML (stars). Dashed vertical lines mark the island base and top. Here, $\Omega_o=\Omega/a_{Si}^3$, where Ω is the average atomic volume as defined in Ref. 53.

In Fig. 6(a), we show 2D contour plots of the hydrostatic stress, p_σ^i, in the plane cutting through the island's apex for three systems with different spacer layer thicknesses: (1) $h_{sp}=81$ ML, (2) $h_{sp}=49$ ML, and (3) $h_{sp}=21$ ML. For small h_{sp} (see the $h_{sp}=21$ ML case), the hydrostatic stress, being compressive outside the area projected by the island base, changes rapidly to tensile, as the apex of the island is approached. As h_{sp} increases, this tendency changes (see the $h_{sp}=81$ ML case), with the hydrostatic stress being now tensile in the region outer than projected by the island base and compressive in the inner region. We note that, in all the investigated cases, a narrow region near the apex of the island remains under a large compressive stress. The hydrostatic stress patterns for different h_{sp} demonstrate noticeable differences in the medium surrounding the QD, even for the two cases where the qualitative behaviors along the x axis are, to a very large extent, similar.

Figure 6(b) shows 2D contour plots of the hydrostatic stress behavior in the planes cutting through the center of the Ge island (at $\simeq$ half of its height) for the same three different spacer layer thicknesses as in Fig. 6(a). In all cases, the hydrostatic stress is highly compressive in the island's interior. Its behavior in the region between the islands varies considerably with h_{sp}; being mildly tensile for large values of h_{sp}, the hydrostatic stress turns compressive as h_{sp} decreases (see the $h_{sp}=21$ ML case). With decreasing values of h_{sp}, the interior of the island experiences considerable stress relaxation with the compressive hydrostatic stress in the island's center going from $\simeq -1.80\times10^9$ J/$\Omega_o m^3$ to $\simeq -1.35\times10^9$ J/$\Omega_o m^3$ as h_{sp} decreases from 81 to 21 ML. Moreover, for a large value of $h_{sp}=81$ ML the hydrostatic stress is nearly flat inside the island, whereas it relaxes considerably towards the center of the island by a factor of $\simeq 0.2\times10^9$ J/$\Omega_o m^3$ for $h_{sp}=21$ ML.

Biaxial stress

While the hydrostatic stress essentially sets the overall energy scale for the valence band energies with respect to the conduction band, the significant part of the valence band confinement potential in QD systems arises from the influence of the biaxial stress (strain). In Fig. 7, we show the biaxial stress, σ_b, variations along the vertical direction (N_z being the atomic plane number with $N_z=0$ for the topmost Si layer of the substrate) passing through the island apex, computed for the same QD systems as above, with three different spacer layer thicknesses, h_{sp}. Similar to the hydrostatic stress,[45] the relaxation of the biaxial stress in the Si(001) substrate, the Ge island, and the spacer layer is spacer thickness dependent. The biaxial stress in the Si(001) substrate is tensile for small spacer layer thicknesses (see $h_{sp}=21$ ML case), while it becomes compressive for the large ones (see $h_{sp}=81$ ML case). In the Ge island interior, the biaxial stress is tensile and large in magnitude ($\simeq 1.6\times10^9$ J/$\Omega_o m^3$). In the spacer layer it suddenly turns compressive for all the investigated spacer layer thicknesses. Note that, unlike in the case of hydrostatic stress, the biaxial stress profiles are not flat inside the Ge island interior for any of the spacer thickness. Furthermore, in all the investigated cases, a $\simeq 0.5\times10^9$ J/$\Omega_o m^3$ decrease in the magnitude is observed towards the island apex. This would lead to corresponding changes in vertical coordinate dependency of the band-edge alignments of the conduction band, with the decreased degree of splitting in the vertical direction observed towards the apex of the Ge island.

The 2D contour plots of the biaxial stress, σ_b, are shown in Fig. 8(a) in the planes cutting through the Ge island's apex for the same three systems with different spacer layer thicknesses: (1) $h_{sp}=81$ ML, (2) $h_{sp}=49$ ML, and (3) $h_{sp}=21$ ML. In all the investigated cases, the biaxial stress is negative in the region around the Ge island apex, suggesting that, for any spacer layer thickness, the relaxation (in the form of expansion) occurs in the lateral (x and y) directions. We note that the behavior of the biaxial stress magnitude is not monotonic with the spacer layer thickness. Thus, in the region surrounding the island's apex, σ_b increases with h_{sp}, for small values of the spacer layer thickness, while a sudden decrease for $h_{sp}=81$ ML is observed. In general, the biaxial stress behavior is characterized by three different regions. In the first region, the biaxial stress is negative and increases rapidly in absolute value towards the island edges. This region corresponds to the island interior, close to the island's apex. The next region is characterized by a decreasing magnitude of the biaxial stress in the direction towards the projected island base edges. In the region between islands, the biaxial stress turns mildly tensile, with a maximum in its magnitude observed approximately near the borders of the projected island base edges. As Fig. 8 (a) shows, the biaxial stress patterns demonstrate an asymmetry along the [100] and $[1\bar{1}0]$ directions, associated with the orientation of island edges.

The 2D contour plots of the biaxial stress, in the planes cutting through the Ge island's center for the same three systems as above, are shown in Fig. 8(b). In all the investi-

gated cases, the interior of the Ge island exhibits a large positive biaxial stress, which homogeneously relaxes towards the center of the system with h_{sp}. Unlike in the case of the hydrostatic stress, the strongest relaxation here is observed in the case of largest h_{sp} (see the $h_{sp}=81$ ML case). In the close vicinity of the Ge island's {105} facets, the biaxial stress turns mildly negative; then it grows with the distance from the island center up to the point approximately corresponding to the projection of the island's base edges. After crossing this point the biaxial stress magnitude monotonically decreases with the distance from the center of the system, approaching zero from above. In general, the variations in the biaxial stress in the lateral direction with the spacer layer thickness are smaller in magnitude as compared to the hydrostatic stress.

VIII. SUMMARY AND CONCLUSIONS

In summary, we have performed atomistic simulations of the systems of buried pyramidal Ge/Si(001) islands with shallow {105} sidewalls and a square base, using a Stillinger-Weber system as a vehicle. We find a strong dependence of the three-dimensional hydrostatic stress distribution, induced by the buried islands, on the spacer thickness. The hydrostatic stress on the spacer layer surface above such an island apex is tensile, and varies as $\sim 1/h_{sp}$ with the spacer layer thickness. The magnitude of the tensile stress field on the spacer layer surface scales approximately with the area of the embedded islands. A comparison of our findings with the experimental data has shown that the inverse linear dependence found in our simulations compares well with the experimentally observed stress behavior. An examination of the atomic displacement fields of the spacer surface atoms has shown that the morphology is nearly planar for intermediate and large spacer layer thicknesses. The variation of the hydrostatic stress in the spacer surface plane reveals a spacer layer thickness dependent tensile region around the island apex that crosses over to compressive stress. The cross-sectional profile of the surface stress thus has the same qualitative ''bell'' shape as produced by the pointlike source force dipole models. We find that the width of the tensile stress region on the spacer layer surface follows a power-law dependence on the spacer layer thickness, with the exponent being $\simeq 1.4$. We provide a calculation of the island vertical alignment energy in a two-layer system of islands which

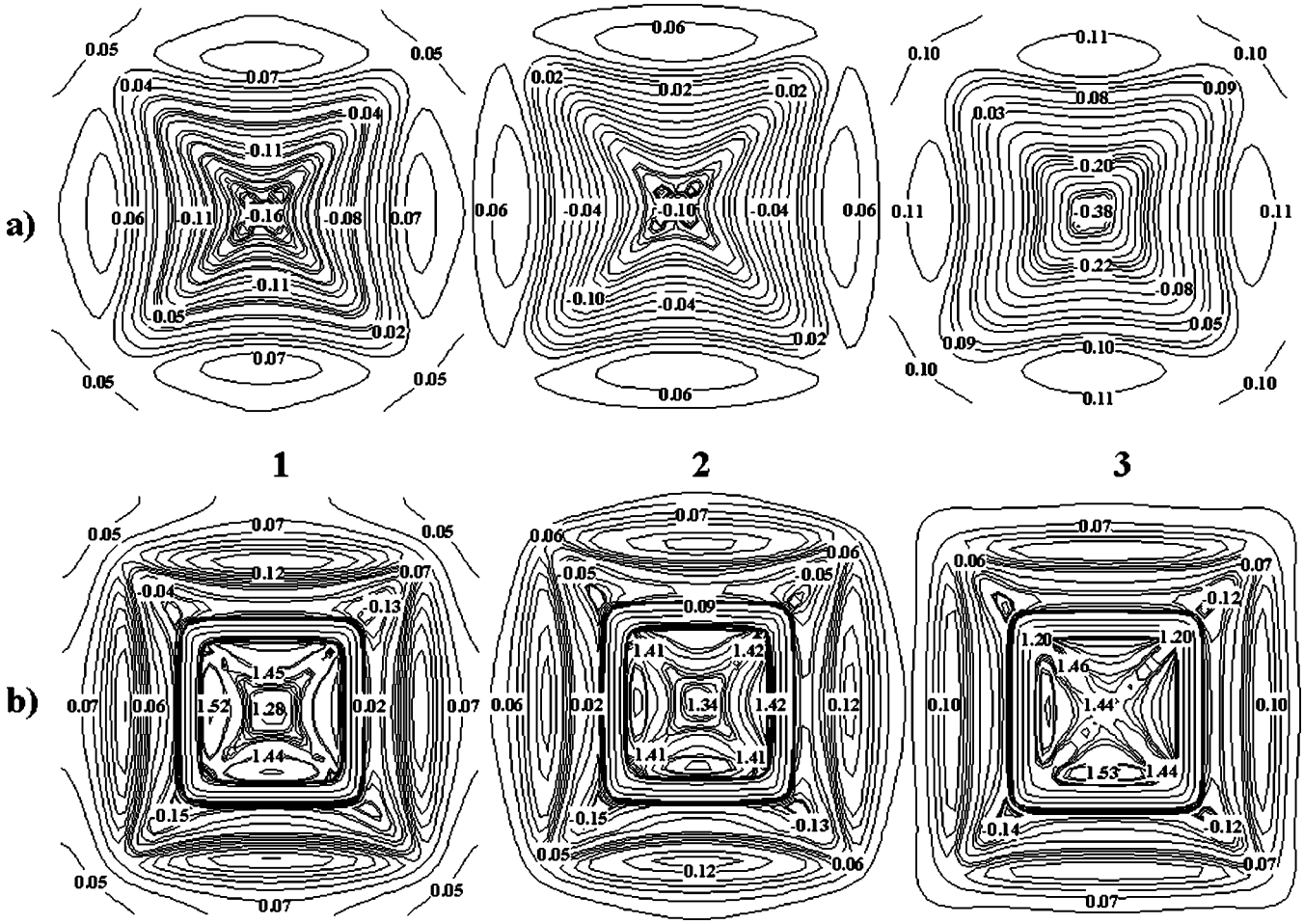

FIG. 8. Contour plots of the biaxial stress (in the units of 10^9 J/$\Omega_o m^3$) in the plane cutting through (a) the island apex and (b) the center of the island are shown for three different spacer layer thicknesses: (1) $h_{sp}=81$ ML, (2) $h_{sp}=49$ ML, and (3) $h_{sp}=21$ ML. Island size is 17 ML.

shows, as expected, that the state of perfect vertical correlation correspond to the elastic energy minimum. The buried island induced hydrostatic and biaxial stress distributions in the interior of Si(001) matrix are examined, given the significance of the former (latter) for defining the conduction (valence) band edge profiles, and hence the three-dimensional confinement potential that turns the island/matrix system into a quantum dot system. The degree of both hydrostatic and biaxial stress relaxation near the island surface at various heights is found to depend strongly on the spacer layer thickness.

ACKNOWLEDGMENTS

This work was supported by the AFOSR under the MURI program. Simulations were performed using the high performance computing facilities at the University of Southern California.

*Email address: makeev@usc.edu

[1] For a recent review, see D. Bimberg, M. Grundmann, and N. N. Ledentsov, *Quantum Dot Heterostructures* (Wiley, Chichester, UK, 1998); V.A. Shchukin and D. Bimberg, Rev. Mod. Phys. **71**, 1125 (1999).

[2] *Self-Assembled InGaAs/GaAs Quantum Dots*, Semiconductors and Semimetals, Vol. 60, edited by M. Sugawara (Academic Press, New York, 1999).

[3] I. Mukhametzhanov, Z. Wei, R. Heitz, and A. Madhukar, Appl. Phys. Lett. **75**, 85 (1999).

[4] Q. Xie, P. Chen, and A. Madhukar, Appl. Phys. Lett. **65**, 2051 (1994).

[5] Q. Xie, A. Madhukar, P. Chen, and N.P. Kobayashi, Phys. Rev. Lett. **75**, 2542 (1995).

[6] N.N. Ledentsov, V.A. Shchukin, M. Grundmann, N. Kirstaedter, J. Böhrer, O. Schmidt, D. Bimberg, V.M. Ustinov, A.Yu. Egorov, A.E. Zhukov, P.S. Kop'ev, S.V. Zaitsev, N.Yu. Gordeev, Zh.I. Alferov, A.I. Borovkov, A.O. Kosogov, S.S. Ruvimov, P. Werner, U. Gösele, and J. Heydenreich, Phys. Rev. B **54**, 8743 (1996).

[7] G.S. Solomon, J.A. Trezza, A.F. Marshal, and J.S. Harris, Jr., Phys. Rev. Lett. **76**, 952 (1996); G.S. Solomon, S. Komarov, J.S. Harris, Jr., and Y. Yamamoto, J. Cryst. Growth **175/176**, 707 (1997).

[8] M.S. Miller, J. Malm, M. Pistol, S. Jeppesen, B. Kowalski, K. Georgesson, and L. Samuelson, J. Appl. Phys. **80**, 3360 (1996).

[9] H.J. Lee, H. Ryu, J.Y. Leam, S.K. Noh, H.G. Lee, and S. Nahm, J. Cryst. Growth **172**, 18 (1997).

[10] Y. Nakata, Y. Sugiyama, T. Futatsugi, and N. Yokoyama, J. Cryst. Growth **175/176**, 713 (1997).

[11] L. Vescan, W. Jäger, C. Dieker, K. Schmidt, A. Hartmann, and H. Lüth, in *Mechanisms of Heteroexpitaxial Growth*, edited by M.F. Chisholm, B.J. Garrison, R. Hull, and L.J. Schowalter, MRS Symposia Proceedings No. 263 (Materials Research Society, Pittsburgh, 1992), p. 23.

[12] B. Rahmati, W. Jäger, H. Trinkaus, R. Loo, L. Vescan, and H. Lüth, Appl. Phys. A: Mater. Sci. Process. **62**, 575 (1996).

[13] C. Teichert, M.G. Lagally, L.J. Peticolas, J.C. Bean, and J. Tersoff, Phys. Rev. B **53**, 16 334 (1996).

[14] A.A. Darhuber, V. Holy, J. Stangl, G. Bauer, A. Krost, F. Heinrichsdorff, M. Grundmann, D. Bimberg, V.M. Ustinov, P.S. Kop'ev, A.O. Kosogov, and P. Werner, Appl. Phys. Lett. **70**, 955 (1997).

[15] P. Schittenhelm, C. Engel, F. Findeis, G. Abstreiter, A.A. Darhuber, G. Bauer, A.O. Kosogov, and P. Werner, J. Vac. Sci. Technol. B **16**, 1575 (1998).

[16] E. Mateeva, P. Sutter, J.C. Bean, and M.G. Lagally, Appl. Phys. Lett. **71**, 3233 (1997).

[17] A.A. Darhuber, P. Schittenhelm, V. Holý, J. Stangl, G. Bauer, and G. Abstreiter, Phys. Rev. B **55**, 15 652 (1997).

[18] O.G. Schmidt, O. Kienzle, Y. Hao, K. Eberl, and F. Ernst, Appl. Phys. Lett. **74**, 1272 (1999).

[19] V. Le Thanh, V. Yam, P. Boucaud, F. Fortuna, C. Ulysse, D. Bouchier, L. Vervoort, and J.-M. Lourtioz, Phys. Rev. B **60**, 5851 (1999).

[20] O.G. Schmidt and K. Eberl, Phys. Rev. B **61**, 13 721 (2000).

[21] O.G. Schmidt, N.Y. Jin-Phillipp, C. Lange, U. Denker, K. Eberl, R. Schreiner, H. Gräbeldinger, and H. Schweizer, Appl. Phys. Lett. **77**, 4139 (2000).

[22] M. Meduna, V. Holy, T. Roch, G. Bauer, O.G. Schmidt, and K. Eberl, J. Phys. D **34**, A193 (2001).

[23] O. Kienzle, F. Ernst, M. Rühle, O.G. Schmidt, and K. Eberl, Appl. Phys. Lett. **74**, 269 (1998).

[24] J. Stangl, A. Daniel, V. Holy, T. Roch, G. Bauer, I. Kegel, T.H. Metzger, Th. Weibach, O.G. Schmidt, and K. Eberl, Appl. Phys. Lett. **79**, 1474 (2001).

[25] K. Eberl, M.O. Lipinski, Y.M. Manz, W. Winter, N.Y. Jin-Phillipp, and O.G. Schmidt, Physica E **9**, 164 (2001).

[26] V. Le Thanh, Surf. Sci. **492**, 255 (2001).

[27] G. Springholz, V. Holy, M. Pinczolits, and G. Bauer, Science **282**, 734 (1998).

[28] V. Holý, G. Springholz, M. Pinczolits, and G. Bauer, Phys. Rev. Lett. **83**, 356 (1999).

[29] G. Springholz, M. Pinczolits, P. Mayer, V. Holy, G. Bauer, H.H. Kang, and L. Salamanca-Riba, Phys. Rev. Lett. **84**, 4669 (2000).

[30] G. Springholz, M. Pinczolits, V. Holy, S. Zerlauth, I. Vavra, and G. Bauer, Physica E **9**, 149 (2001).

[31] I.L. Krestnikov, M. Strassburg, M. Caesar, A. Hoffmann, U.W. Pohl, D. Bimberg, N.N. Ledentsov, P.S. Kop'ev, Zh.I. Alferov, D. Litvinov, A. Rosenauer, and D. Gerthen, Phys. Rev. B **60**, 8695 (1999).

[32] J. Tersoff, C. Teichert, and M.G. Lagally, Phys. Rev. Lett. **76**, 1675 (1996).

[33] F. Liu, S.E. Davenport, H.M. Evans, and M.G. Lagally, Phys. Rev. Lett. **82**, 2528 (1999).

[34] S. Christiansen, M. Albrecht, H.P. Strunk, and H.J. Maier, Appl. Phys. Lett. **64**, 3617 (1994).

[35] T. Benabbas, P. Francois, Y. Androussi, and A. Lefebvre, J. Appl. Phys. **80**, 2763 (1996); T. Benabbas, Y. Androussi, and A. Lefebvre, J. Appl. Phys. **86**, 1945 (1999).

[36] G. Muralidharan, Jpn. J. Appl. Phys. **39**, L658 (2000).

[37] A.E. Romanov, G.E. Beltz, W.T. Fischer, P.M. Petroff, and J.S. Speck, J. Appl. Phys. **89**, 4523 (2001).

[38] V.A. Shchukin, D. Bimberg, V.G. Malyshkin, and N.N. Ledentsov, Phys. Rev. B **57**, 12 262 (1998).

[39] V.A. Shchukin, N.N. Ledentsov, and D. Bimberg, Physica E **9**, 140 (2001).
[40] W. Yu and A. Madhukar, Phys. Rev. Lett. **79**, 905 (1997); **79**, 4939(E) (1997).
[41] W. Yu and A. Madhukar, in *Proceedings of the 23rd International Conference on Physics of Semiconductors, Berlin, Germany*, 1996, edited by M. Scheffler and R. Zimmermann (World Scientific, Singapore, 1996), Vol. 2, p. 1309.
[42] I. Daruka, A.-L. Barabási, S.J. Zhou, T.C. Germann, P.S. Lomdahl, and A.R. Bishop, Phys. Rev. B **60**, R2150 (1999).
[43] Y. Kikuchi, H. Sugii, and K. Shintani, J. Appl. Phys. **89**, 1191 (2001).
[44] A.V. Nenashev and A.V. Dvurechenskii, Zh. Éksp. Teor. Fiz. **118**, 570 (2000) [JETP **91**, 497 (2000)].
[45] M.A. Makeev and A. Madhukar, Phys. Rev. Lett. **86**, 5542 (2001).
[46] C. Kohler, J. Phys.: Condens. Matter **15**, 133 (2003).
[47] Y.-W. Mo, D.E. Savage, B.S. Swartzentruber, and M.G. Lagally, Phys. Rev. Lett. **65**, 1020 (1990).
[48] H. Balamane, T. Halicioglu, and W.A. Tiller, Phys. Rev. B **46**, 2250 (1992).
[49] F.H. Stillinger and T.A. Weber, Phys. Rev. B **31**, 5262 (1985).
[50] K. Ding and H.C. Andersen, Phys. Rev. B **34**, 6987 (1986).
[51] J. Zi, K. Zhang, and X. Xie, Phys. Rev. B **41**, 12 915 (1990).
[52] C. Roland and G.H. Gilmer, Phys. Rev. B **47**, 16 286 (1993).
[53] R.J. Hardy, J. Chem. Phys. **76**, 622 (1982); V. Vitek and T. Egami, Phys. Status Solidi B **144**, 145 (1987).
[54] J.F. Lutsko, J. Appl. Phys. **65**, 2991 (1989).
[55] W.W. Mullins, J. Appl. Phys. **28**, 333 (1957).
[56] C.-S. Lee, B. Kahng, and A.-L. Barabasi, Appl. Phys. Lett. **78**, 984 (2001).
[57] T. Mura, In *Micromechanics of Defects in Solids* (Martinus Nijhoff, Hague, The Netherlands, 1984).
[58] A.E.H. Love, *Mathematical Theory of Elasticity* (Cambridge University Press, Cambridge, England, 1927).
[59] S. Timoshenko, *Theory of Elasticity* (McGraw-Hill, New York, 1934).
[60] R.D. Mindlin, Physics **7**, 195 (1936).
[61] R.D. Mindlin and D.H. Cheng, J. Appl. Phys. **21**, 926 (1950).
[62] R.D. Mindlin and D.H. Cheng, J. Appl. Phys. **21**, 930 (1950).
[63] A.A. Maradudin and R.F. Wallis, Surf. Sci. **91**, 423 (1980).
[64] J.N. Goodier, Philos. Mag. **7**, 1017 (1937).
[65] J.D. Eshelby, J. Appl. Phys. **25**, 255 (1954); Solid State Phys. **3**, 79 (1956).
[66] S.M. Hu, J. Appl. Phys. **66**, 2741 (1989).
[67] S.M. Hu, J. Appl. Phys. **70**, R53 (1991).
[68] M.A. Makeev and A. Madhukar, Phys. Rev. B **67**, 073201 (2003).
[69] The inadequacy of the h_{sp}^{-3} power dependence also suggests that those parts of the analysis in Ref. 20 that relied upon the usage of Eq. (2) of Ref. 20 are in need of re-examination.
[70] G.L. Bir and G.E. Pikus, *Symmetry and Strain-Induced Effects in Semiconductors* (Nauka, Moscow, 1972; Wiley, Halsted, UK, 1974).
[71] J.C. Hensel and G. Feher, Phys. Rev. **129**, 1041 (1963).
[72] H. Hasegawa, Phys. Rev. **129**, 1029 (1963).
[73] F.H. Pollak and M. Cardona, Phys. Rev. **172**, 816 (1968).
[74] C.G. Van de Walle, Phys. Rev. B **39**, 1871 (1989).
[75] M. Grundmann, O. Stier, and D. Bimberg, Phys. Rev. B **52**, 11 969 (1995); **58**, 10 557 (1998); O. Stier, M. Grundmann, and D. Bimberg, *ibid.* **59**, 5688 (1999).
[76] M.A. Cusack, P.R. Briddon, and M. Jaros, Phys. Rev. B **54**, R2300 (1996).
[77] T. Saito, J.N. Schulman, and Y. Arakawa, Phys. Rev. B **57**, 13 016 (1998).
[78] C. Pryor, J. Kim, L.W. Wang, A.J. Williamson, and A. Zunger, J. Appl. Phys. **83**, 2548 (1998).
[79] L.-W. Wang, J. Kim, and A. Zunger, Phys. Rev. B **59**, 5678 (1999); A.J. Williamson and A. Zunger, *ibid.* **59**, 15 819 (1999); A.J. Williamson, L.W. Wang, and A. Zunger, *ibid.* **62**, 12 963 (2000).
[80] S.J. Sun and Y-C. Chang, Phys. Rev. B **62**, 13 631 (2000).
[81] O.G. Schmidt, K. Eberl, and Y. Rau, Phys. Rev. B **62**, 16 715 (2000).
[82] J.H. Seok and J.Y. Kim, Appl. Phys. Lett. **78**, 3124 (2001).
[83] M. Yang, J.C. Sturm, and J. Prevost, Phys. Rev. B **56**, 1973 (1997).